SAPIENZA
UNIVERSITÀ DI ROMA

Vehicle Systems Dynamics

Aircraft Landing Gear: Simulation and Control

A.Mauro E.Nicotra M.Azeez

Dipartimento di Ingegneria Informatica Automatica e Gestionale
Antonio Ruberti
Control Engineering
Sapienza Università di Roma

Academic year 2020/2021

Professor A. Carcaterra & G. Pepe

Contents

1 Introduction

The focus of this work is the development of a Multi-degree of freedom model for simulation and control of the landing performances of an airplane. From dynamic considerations, the landing gear performance has two areas of interest: the behaviour during touchdown impact, and the response to excitation induced by track roughness during taxi, take-off and landing runs. The high level of transients induced during touchdown have to be controlled smoothly in order to achieve the steady state in a reasonable amount of time.
A 4-dof model is derived considering the dynamics of the wheels of the airplane and the landing gears. The latter is then augmented with three additional degrees of freedom in order to consider also the horizontal coordinate and the wheels angular velocity. Analyses with and without the runway profile are carried out to study the effects of the input signals on the derived model.
The controlled variable are the elevators, the flaps and the active suspension of the front landing gear, and due to the high nonlinearity of the system, in place of using a linear controller derived from the linearized system, the Variational Feedback Controller is implemented on the latter. Moreover, the two additional inputs are relative to the brakes of the rear and the front wheels

1.1 Landing Simulation

The focus of the project can be divided in three cases of interest:

1. the simulation starts with the airplane flying a few hundred meters above the ground, this initial phase ends when the rear wheels touch the ground

2. the second phase starts when the rear wheels have just touched the runway, and continues until the nose wheel touches the runway too

3. the last phase starts when the nose wheel touches the runway, and continues until the aircraft comes to a constant linear velocity, completing the transition from flying to taxiing, or eventually until it stops

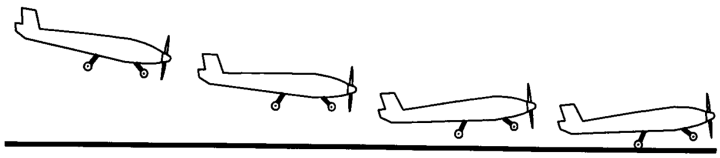

Figure 1: Stages of landing

1.2 Overview of Landing Gears

The landing gear is the critical component for what concerns the aircraft ground-maneuvers such as taxi, take-off and landing. In particular the landing is the most important since it involves a massive amount of energy transfer and the system has to be stable enough to operate under these conditions. Then there are some constraints and requirements for the performance of the landing gears such as crash survivability, riding performance, weight, height, steering and so on.
Although there are so many different variants of the model, the conventional landing gear has a

tired wheel unit, a shock absorbing unit and a supporting structure. The wheel unit has a main wheel assembly attached to the fuselage and a nose wheel assembly attched to the nose of the aircraft.
During the landing, the main wheels come in contact with the ground first which is called the touchdown and then the nose wheel makes contact with the ground.
The geometry of the nose wheel is important too, and many variants exist. In this project the semi-articulated (fig. 2) model has been adopted, in particular all the displacement have been considered as parallel to the vertical direction, since they can always be derived with geometric considerations. This allows to model the landing gears as the well-known suspension model of the quarter-vehicle.

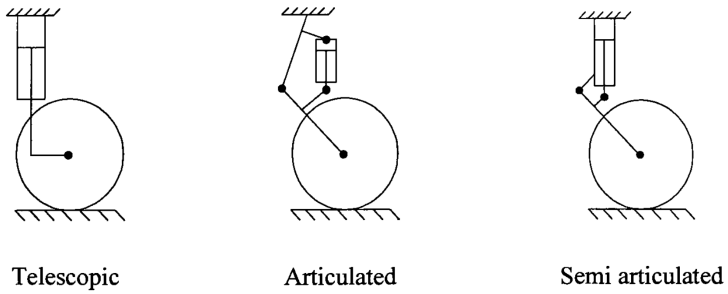

Figure 2: Types of landing gears

Usually the main landing gear carries about 85% of total weight of aircraft while the front gear carries around 12-15% of the weight of the aircraft, which causes the center of gravity of the aircraft to be in the proximity of the main landing gear, and consequently the equilibrium position of the pitch angle is slightly more than zero degrees.

2 Aircraft Model

Given the scope of this study is to control the vertical velocity, the pitch angle and the suspension systems upon landing, our model needs to include the dynamics of the aircraft landing gears. The landing gear comprises the suspension systems that provide the smooth ride and provide the principal support to the airplane during landing. They also absorb the landing impact energy so as to minimize the loads transmitted to the air-frame and damp oscillations caused by road bumps. For these reasons our model is primarily focused on the dynamics of the suspensions systems of the nose and main landing gear and that of the pitch angle. The model for the landing gears makes reference to the quarter-vehicle model which are widely used in vehicle and suspension analyses.

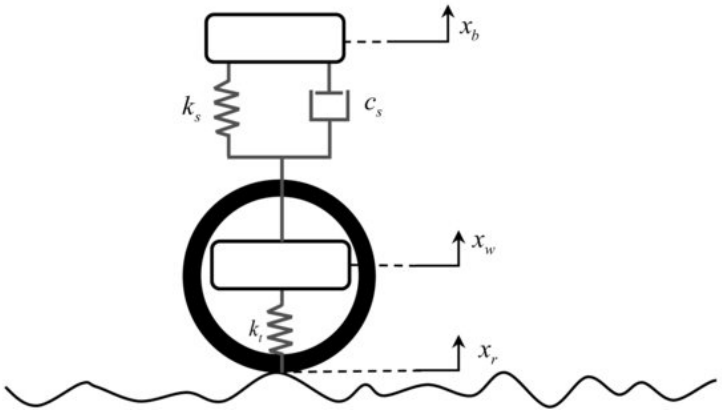

Figure 3: Diagram of Quarter car model

In particular, The system taken into consideration is a seven degree of freedom system for which we have a differential equation to describe the motion of each one of them. Consider the following diagram as a descriptive image of our system which will be useful as we begin to derive each of the equations of motion through Newton's second law of motion.

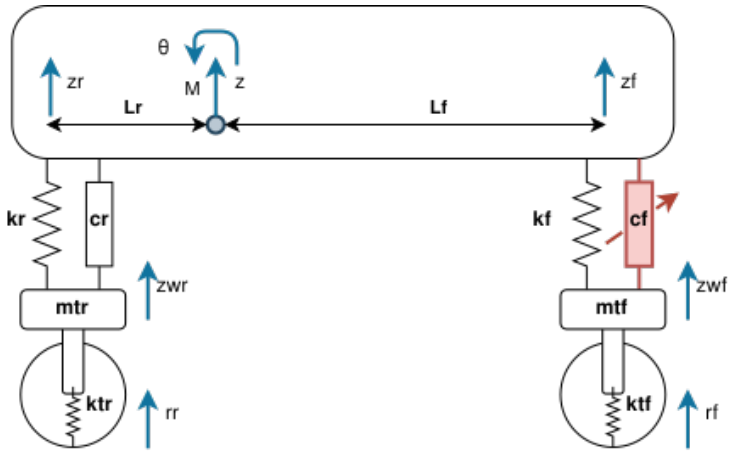

Figure 4: Diagram illustrating coordinates of interest

The mass of the fuselage of the aircraft is considered as the sprung mass M of the system with vertical displacement (z). The quantities z_f and z_r represents the vertical coordinates where the

front and rear landing gears act on the sprung mass with them both sharing a dependence on θ which will be illustrated below.

$$z_f = z + l_f \sin\theta$$
$$z_r = z - l_r \sin\theta$$

And their respective derivatives being:

$$\dot{z_f} = \dot{z} + l_f \dot{\theta} \cos\theta$$
$$\dot{z_r} = \dot{z} - l_r \dot{\theta} \cos\theta$$

The nose and main wheels are also modeled as spring mass systems with masses m_t and spring constants k_t which represents the elasticity of the tires. While z_{wr} and z_{wf} represents the vertical displacement of the center of the main wheel and that of the front wheel.
Now let us consider z; the forces acting on the fuselage to cause a displacement on z are the forces from the front and rear landing gears.
Newton's law allows us to write the following :

$$M\ddot{z} = F_{kf} + F_{cf} + F_{kr} + F_{cr} + F_g \tag{1}$$

The signs of the forces are determined by the direction of z, with F_g being the force of gravity, $F_{kf} = -k_f(z_f - z_{wf})$ and $F_{cf} = -c_f(\dot{z_f} - \dot{z_{wf}})$ respectively representing the elastic force originated from spring k_f and the variable damping force from the shock absorber. The same case applies symmetrically for the forces on the rear landing gear with $F_{kr} = -k_r(z_r - z_{wr})$ and $F_{cr} = -c_r(\dot{z_r} - \dot{z_{wr}})$.
Combining these forces we obtain

$$M\ddot{z} = -k_f(z_f - z_{wf}) - c_f(\dot{z_f} - \dot{z_{wf}}) - k_r(z_r - z_{wr}) - c_r(\dot{z_r} - \dot{z_{wr}}) - Mg \tag{2}$$

With c_f representing the control variable of the equation, since we are dealing with semi active suspension systems.
Now to obtain the equation of the the front landing gear (z_{wf}) which is symmetrical to that of the rear landing gear, we can write the following equation thanks to Newton's law:

$$m_{tf}\ddot{z}_{wf} = F_{kf} + F_{cf} + F_{ktf} \tag{3}$$

Aforementioned, the signs of the forces depend on the direction chosen for z_{wf}, in particular $F_{kf} = k_f(z_f - z_{wf})$, $F_{cf} = c_f(\dot{z}_f - \dot{z}_{wf})$ and $F_{ktf} = -k_{tf}(z_{wf} - r_f)$. For which combined we have the following:

$$m_{tf}\ddot{z}_{wf} = k_f(z_f - z_{wf}) + c_f(\dot{z}_f - \dot{z}_{wf}) - k_{tf}(z_{wf} - r_f) \tag{4}$$

The same analysis is symmetrical to the rear landing gear case for which we have the following equation:

$$m_{tr}\ddot{z_{wr}} = k_r(z_r - z_{wr}) + c_r(\dot{z_r} - \dot{z_{wr}}) - k_{tr}(z_{wr} - r_r) \tag{5}$$

To describe the motion of θ, we consider the torques applied on the fuselage by both landing gears.

A free body diagram to illustrate the orientation of θ and the sense of the torques of the system can be found in figure 3
If we denote $F_f = -k_f(z_f - z_{wf}) - c_f(\dot{z_f} - \dot{z_{wf}})$ and $F_r = -k_r(z_r - z_{wr}) - c_r(\dot{z_r} - \dot{z_{wr}})$.
We can write the following using Newton's law :

$$J\ddot{\theta} = -(k_f l_f)(z_f - z_{wf}) - (c_f l_f)(\dot{z}_f - \dot{z}_{wf}) + (k_r l_r)(z_r - z_{wr}) + (c_r l_r)(\dot{z}_r - \dot{z}_{wr}) \tag{6}$$

J represents the moment of inertia of the fuselage, $\ddot{\theta}$ the angular acceleration of θ, considered positive if counter-clockwise. Finally Adding a pitch moment Ju_θ as a control variable, we get the following equation :

$$J\ddot{\theta} = -(k_f l_f)(z_f - z_{wf}) - (c_f l_f)(\dot{z}_f - \dot{z}_{wf}) + (k_r l_r)(z_r - z_{wr}) + (c_r l_r)(\dot{z}_r - \dot{z}_{wr}) + Ju_\theta \tag{7}$$

The chosen orientation for θ and sense of the torques are illustrated in Fig 5.

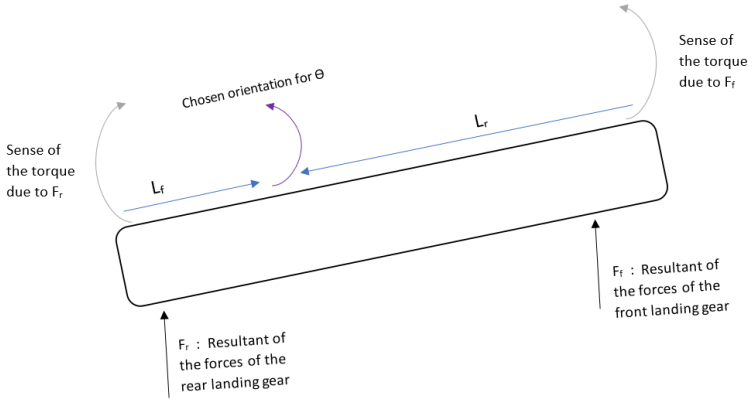

Figure 5: Orientation of θ

Eventually, the combination of the the four equations yields to:

$$\ddot{z} = -\frac{1}{M}\left[k_f(z_f - z_{wf}) + c_f(\dot{z}_f - \dot{z}_{wf}) + k_r(z_r - z_{wr}) + c_r(\dot{z}_r - \dot{z}_{wr}) + L\right] - g \tag{8}$$

$$\ddot{z}_{wf} = \frac{1}{m_t}\left[k_f(z_f - z_{wf}) + c_f(\dot{z}_f - \dot{z}_{wf}) - k_t(z_{wf} - y_f)\right] - g \tag{9}$$

$$\ddot{z}_{wr} = \frac{1}{m_t}\left[k_r(z_r - z_{wr}) + c_r(\dot{z}_r - \dot{z}_{wr}) - k_t(z_{wr} - y_r)\right] - g \tag{10}$$

$$\ddot{\theta} = \frac{1}{J}\left[-(k_f l_f)(z_f - z_{wf}) - (c_f l_f)(\dot{z}_f - \dot{z}_{wf}) + (k_r l_r)(z_r - z_{wr}) + (c_r l_r)(\dot{z}_r - \dot{z}_{wr}) + u_\theta\right] \tag{11}$$

2.1 Pacejka Model

In addition to the four equations presented above, it is necessary also to take into account the dynamics along the horizontal direction x. To this end it is necessary to consider the tires dynamics, hence in total three more equation are added to the model, one for the horizontal coordinate x and the other two for the tire angular velocities ω_f and ω_r, yielding to an augmented system of a total of seven degrees of freedom and seven differential equations.
In order to write down the equations that describe the dynamics of the wheels, we have decided to apply the Pacejka model. Professor Hans Pacejka developed a series of tire design models which are also named the "Magic Formula" because there is no particular physical basis for the structure of the equations chosen, but they fit a wide variety of tire constructions and operating conditions. These models describe the interaction between the tire tread and road pavement and the main output is the longitudinal force F_{long} arising from this interaction, which is a function of the vertical force F_z and the Pacejka coefficient k, the model is indeed an empirical equation based on four fitting coefficients.

$$F_{long} = D \sin C \arctan(B(1-E)k + E \arctan(Bk)) \tag{12}$$

$$k = -\left(\frac{v_x - \omega R_t}{|v_x|}\right) \cdot 100 \tag{13}$$

where:

1. $B = \dfrac{a_3 F_z^2 + a_4 F_z}{CD \exp\{a_5 F_z\}}$
2. $C = a_0$
3. $D = a_1 F_z^2 + a_2 F_z$
4. $E = a_6 F_z^2 + a_7 F_z + a_8$

and the parameters values are $a_0 = 1.65, a_1 = -21.3, a_2 = 1144, a_3 = 49.6, a_4 = 226, a_5 = 0.069, a_6 = -0.006, a_7 = 0.056$ and $a_8 = 0.486$.
The wheels dynamics equation can be written by applying the Newton's law for the torques acting on each wheel. In this case, in addition to the moment generated from the longitudinal force given by the Pacejka model, namely $F_{long} R_t$, where R_t is the wheel radius, we have considered also a braking moment C_f for the front wheel and C_r for the rear. Finally, also a friction term is added to the model in order to take into account the rolling resistance of the two wheels, C_{roll_f} and C_{roll_r} respectively. Considering the angle with respect to the vertical direction being zero, the latters can be written as

$$C_{roll} = (\mu_0 + \mu_1 \omega^2 R_t^2) F_z R_t \tag{14}$$

with $\mu_0 = 0.015$ and $\mu_1 = 7 \cdot 10^{-6}$.
Being the problem completely planar (xz plane), we have omitted the presence of a lateral velocity V_y, so that the gyroscopic effects can be neglected. It follows that the horizontal acceleration $\ddot{x}$ is given only by the derivative of the velocity V_x, while the force acting in this direction are only the two longitudinal forces F_{long_f} and F_{long_r}, in addition to the viscous resistance due to the air

$$F_{aereo} = \frac{1}{2} \rho_{air} A_x c_d V_x^2 \tag{15}$$

where ρ_{air} is the density of the air, A_x is the area of the plane seen from the front and c_d is the drag coefficient.
In conclusion the three equations are the following:

$$\ddot{x} = \frac{1}{M}(F_{long_r} + F_{long_f} - F_{aereo}) \tag{16}$$

$$\dot{\omega}_r = \frac{1}{I_{wr}}(C_r - F_{long_r R_t} - C_{roll_r}) \tag{17}$$

$$\dot{\omega}_f = \frac{1}{I_{wf}}(C_f - F_{long_f R_t} - C_{roll_f}) \tag{18}$$

where I_{wr} and I_{wf} are the inertia moments of the wheels.
The two systems are coupled by the Pacejka function $F_{long} = f(F_z, k)$ where the vertical forces acting on the wheels come from of the equations 9 and 10 and generate the longitudinal forces for the Pacejka subsystem

3 Road Profile Model

A road pavement can be realized in different ways and using various materials, but in every case, its surface is never perfectly flat, even, and smooth. A proper characterization of road irregularities is an essential issue since they cause airplane vibrations while taxi. This issue can be solved by measuring the profile of the real road (directly by using profilometers or by using dynamic road response devices) or generating an artificial profile with the specified parameters. The main limitation of the experimental methods is the difficulty in obtaining all profiles corresponding to the full range of possible variations, defined by the ISO 8608 standard. To describe the road profile it uses the degree of roughness $G_d(n_o)$ identified as power spectral density (PSD) [Fig. 6] of the vertical road profile displacement and the waviness w. The road profile are classified as belonging to one of the classes (A-H) provided by the ISO 8608 on the basis of $G_d(n_o)$ parameter values while keeping w=2 constant [Fig. 6]. The generation of artificial road profiles allows bypassing difficulties to collect a full set of real road profiles but can contain significant deviations from real one.s There exist several methods (shaping filter, superposition of harmonics, ...) to generate an artificial road profiles conforming the desired ISO classification. In this project we use a method based on linear filtering (13) called white noise filtration.

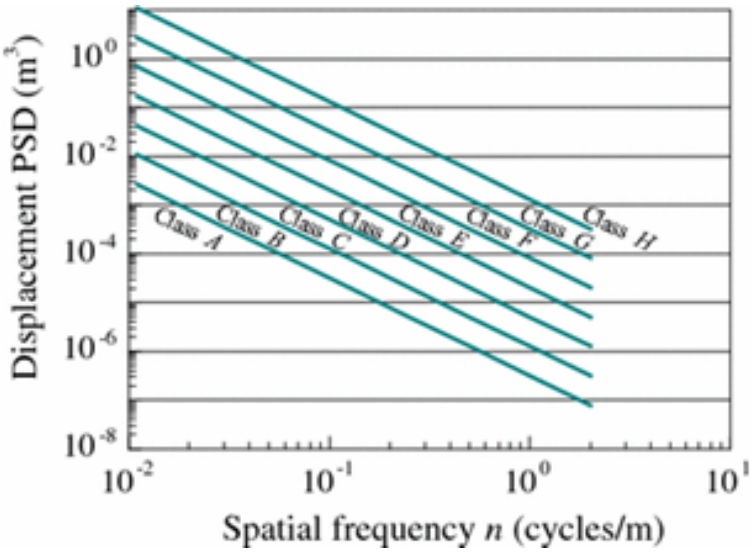

Figure 6: ISO 8608 road profile PSD

For our purpose we want to generate a road profile compliant with the profile corresponding to the ISO 8608 Class B:

$$G_d(k) = G_d(k_o)(\frac{-k}{k_o})^{-w} \tag{19}$$

with w=2, $G_d(k_o) = 4 * 10^{-6} m^3, k_o = 1\frac{rad}{m}$
According to the ISO standard there is no reason to measure spatial frequencies lower than $n_L = 0.01 cycles/m$ for on-road vehicles. For the vibration analysis has suggested an upper spatial frequency limit of $n_U = 10 cycles/m$ by considering the low pass filtering effect due to the tire enveloping. This correspond to a range of $2\pi 0.01 \leq k \leq 2\pi 10$ for the spatial angular frequency.

3.1 White Noise Filtration

A white noise signal can be transformed to the road profile either in the spatial or time domain through a first-order linear shape filter. To avoid an increment on the standard deviation during the integration period the road roughness PSD used in ISO 8608 was modified as:

$$G_d(\omega) = \frac{2\alpha v\sigma^2}{\pi}\frac{1}{\alpha v^2 + \omega^2} \tag{20}$$

$$G_d(k) = \frac{2\alpha\sigma^2}{\pi}\frac{1}{\alpha + k^2} \tag{21}$$

where σ^2 is the road roughness variance, v is the horizontal airplane velocity, ω is the angular frequency in time domain (rad/s) while k is the angular spatial frequency (rad/m). The parameter α is independent of the road and it is termed as a low frequency cut off (rad/m). If the velocity v is constant, then the road profile r(t) with the PSD defined in (11) and (12) can be obtained from the output of a linear shape filter expressed by the differential equation:

$$\frac{dr(t)}{dt} = -\alpha v r(t) + \eta(t) \tag{22}$$

where $\eta(t)$ is a zero-mean Gaussian white noise (m/s) with a PSD of $2\alpha v\sigma^2$. In the spatial domain, (13) can be expressed as: $\frac{\partial r}{\partial x} = -\alpha r(x) + \eta(x)$ where $\frac{\partial r}{\partial x} = \frac{1}{v}\frac{dr}{dt}$
where $\eta(x)$ is a zero mean Gaussian white noise (m/m) and x is the distance travelled by the airplane along the road. In our case, the variance was chosen at $\sigma^2 = 4G_d(k_0)$ with the reference value of PSD $k_0 = 1rad/m$ given by ISO 8608. To generate the road profile [Fig. 8], the white noise filtration method is used the Simulink model [Fig. 7] by using the band-limited white noise block. The ideal white noise cannot be generated numerically due to its infinite variance but an approximation of it is useful for the simulation. To get a one-sided averaged PSD should be $2\pi\alpha v\sigma^2$. Then, the value of parameter α is equal to $\alpha = 0.127rad/m$

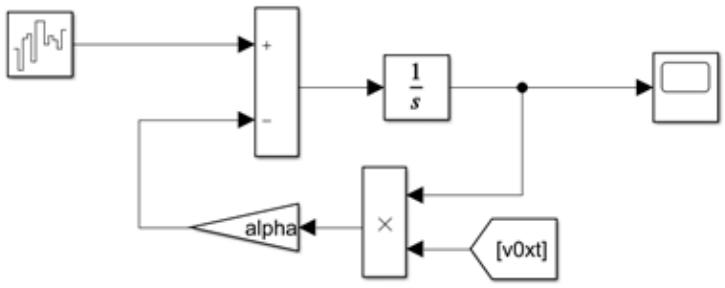

Figure 7: Simulink model

To accommodate the lowest frequency harmonic k_L, the required length of road will be $L \geq \frac{1}{k_L} = 100m$.
According to the sampling theorem, the required step size of x will be $\Delta x \leq \frac{1}{2n_U}$=$0.05m$. In this case, the sampling time is equal to $\frac{1}{2n_U v}$ for our model in Simulink. For a smoother profile, a smaller step can be chosen, but it will cause an increase in the required computational efforts.

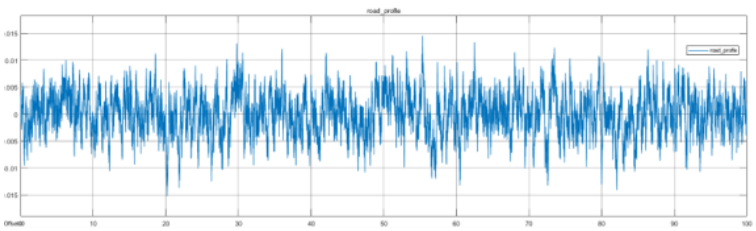

Figure 8: Road Profile

The white noise filtration method easily provides a nice and suitable output since it uses only two variables: the variation σ^2 and low-frequency boundary α. The method is simple, but in the case of unadjusted parameter values, the profile floats away and therefore, the roughness amplitude and period draughts away. This method is sensitive to the virtual driving velocity, as well. The positive side in this method is that the variation σ^2 fits the road profile with $\omega = 2$, according to the corresponding ISO standard. This method does not generate an identical profile picture for every 100m of road profile, as it happens using the method of harmonic functions.

4 Elevator and Flap Control

In this section the elevator and the flaps are presented, firstly by explaining their functioning and then by making a deep analysis on the feedback linearization which has been applied to them.
In the following figures are resumed the three fundamental angle that are used to describe the airplane dynamics.

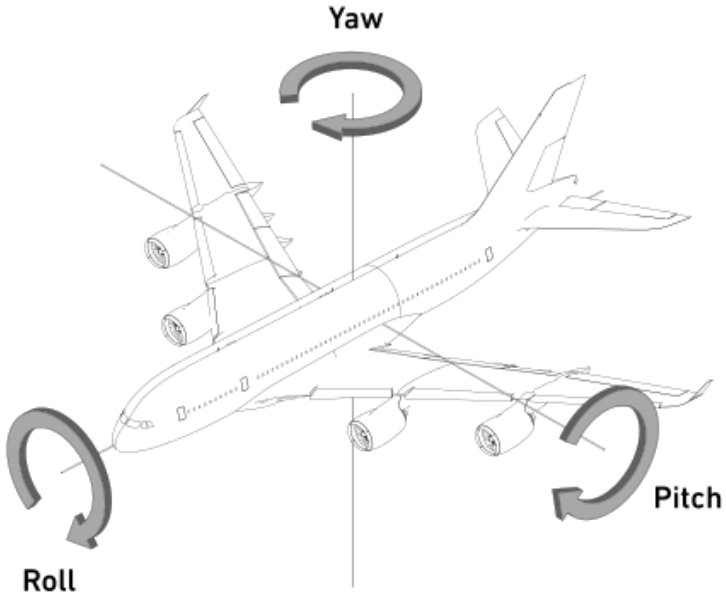

Figure 9: Airplane dynamics angles

4.1 Elevator

An aircraft stabilizer is an aerodynamic surface, typically including one or more movable control surfaces,that provides longitudinal (pitch) and/or directional (yaw) stability and control. A stabilizer can feature a fixed or adjustable structure on which any movable control surfaces are hinged, or it can itself be a fully movable surface such as a stabilator. Depending on the context, "stabilizer" may sometimes describe only the front part of the overall surface.
The empennage, also known as the tail or tail assembly, is a structure at the rear of an aircraft that provides stability during flight.
In particular, in the conventional aircraft configuration, separate vertical (fin) and horizontal (tailplane) stabilizers form an empennage positioned at the tail of the aircraft.
Elevators are flight control surfaces, usually at the rear of an aircraft, which control the aircraft's pitch, and therefore the angle of attack and the lift of the wing. The elevators are usually hinged to the tailplane or horizontal stabilizer.

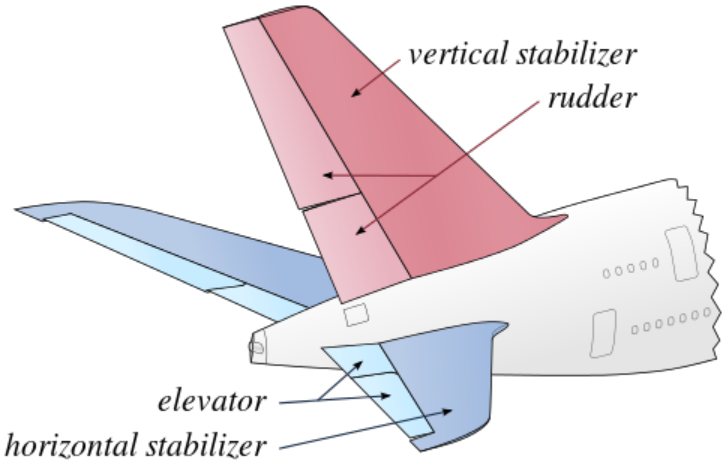

Figure 10: Tail of conventional aircraft

The elevator is a usable up and down system that controls the plane, horizontal stabilizer usually creates a downward force which balances the nose down moment created by the wing lift force, which typically applies at a point (the wing center of lift) situated aft of the airplane's center of gravity. The effects of drag and changing the engine thrust may also result in pitch moments that need to be compensated with the horizontal stabilizer.
Both the horizontal stabilizer and the elevator contribute to pitch stability, but only the elevators provide pitch control. They do so by decreasing or increasing the downward force created by the stabilizer:

1. an increased downward force, produced by up elevator, forces the tail down and the nose up. At constant speed, the wing's increased angle of attack causes a greater lift to be produced by the wing, accelerating the aircraft upwards. The drag and power demand also increase;

2. a decreased downward force at the tail, produced by down elevator, causes the tail to rise and the nose to lower. At constant speed, the decrease in angle of attack reduces the lift, accelerating the aircraft downwards.

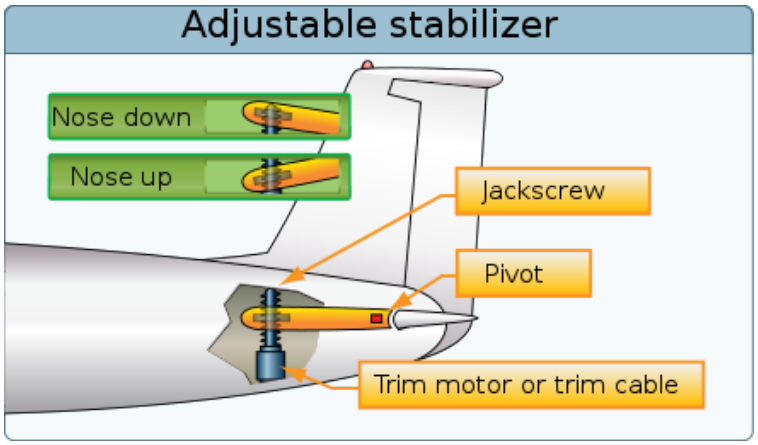

Figure 11: Adjustable stabilizer

Given the equations of motion in (11), the elevator control is focused on the dynamics of the pitch angle, namely $\theta(t)$.
Given the high non-linearity of the equation for $\theta(t)$, the first step to control the pitch angle consists in using the feedback linearization strategy in order to compesate all the nonlinear terms, and eventually use the controller to impose the desired error dynamics.
In the most general form the feedback linearization may be applied to nonlinear systems of the form

$$\begin{aligned} \dot{x} &= f(x) + g(x)u \\ y &= h(x) \end{aligned}$$

where $x \in \mathbb{R}^n$ is the state vector, $u \in \mathbb{R}^p$ is the vector of inputs and, $y \in \mathbb{R}^m$ is the vector of outputs.
The goal is to develop a control input

$$u = \alpha(x) + \beta(x)v \tag{23}$$

that renders a linear input-output map between the new input v and the output.
Since, in this case the model has been restricted to the equation of $\theta(t)$ only, which is exactly the output we want to control, the feedback linearization can be applied straightforwardly, without involving Lie derivatives or further output derivatives, as follows.
The equation can be written as

$$\ddot{\theta} = f(z, z_{wf}, z_{wr}, \dot{z}, \dot{z}_{wf}, \dot{z}_{wr}) + u_\theta \tag{24}$$

where $f(\cdot) = \frac{1}{J}\left[k_r(z - z_{wr}) + c_r(\dot{z} - \dot{z_{wr}} - k_f(z - z_{wf}) + c_f(\dot{z} - \dot{z_{wf}}\right]$ and u_θ is the pitch moment given by the elevator, which actually is a pitch acceleration if divided by the moment of inertia J.
Assuming to use a full state feedback, so by measuring the plane altitude and velocity for the center of mass and the wheels, the control input can be chosen as follows:

$$u_\theta = -f(z, z_{wf}, z_{wr}, \dot{z}, \dot{z}_{wf}, \dot{z}_{wr}) - v \tag{25}$$

The closed-loop system becomes:

$$\ddot{\theta} = f(z, z_{wf}, z_{wr}, \dot{z}, \dot{z}_{wf}, \dot{z}_{wr}) - f(z, z_{wf}, z_{wr}, \dot{z}, \dot{z}_{wf}, \dot{z}_{wr}) - v \tag{26}$$

Then

$$\ddot{\theta} + v = 0 \tag{27}$$

Eventually, the controller term v can be used in order to assign the desired error dynamics.
Given a desired pitch angle $\theta_d(t)$ and a desired angular velocity $\dot{\theta}_d(t)$, the error the be defined as

$$e = \theta - \theta_d \tag{28}$$

and its derivative is

$$\dot{e} = \dot{\theta} - \dot{\theta_d} \tag{29}$$

At this point v can be used to implement a PID controller in the new linearized system by choosing

$$v = K_p e(t) + K_i \int_0^t e(\tau) d\tau + K_d \dot{e}(t) \tag{30}$$

yielding the following closed-loop dynamics

$$\ddot{e} + K_d \dot{e} + K_p e + K_i \int_0^t e(\tau) d\tau = 0 \tag{31}$$

Note that, since $\ddot{\theta}_d = 0$, it follows that $\ddot{\theta} = \ddot{e}$.
With a proper choice for the gains K_p, K_i and K_d the error dynamics can be adjusted according to the desired specifications, such as the settling time, the overshoot and so on.

4.2 Flaps

In aircraft design and aerospace engineering, a high-lift device is a component or mechanism on an aircraft's wing that increases the amount of lift produced by the wing. The device may be a fixed component, or a movable mechanism which is deployed when required.
A flap is a high-lift device used to reduce the stalling speed of an aircraft wing at a given weight. Flaps are usually mounted on the wing trailing edges of a fixed-wing aircraft. Flaps are used to reduce the take-off distance and the landing distance. Flaps also cause an increase in drag so they are retracted when not needed.
Extending the wing flaps increases the camber or curvature of the wing, raising the maximum lift coefficient or the upper limit to the lift a wing can generate. This allows the aircraft to generate the required lift at a lower speed, reducing the minimum speed (known as stall speed) at which the aircraft will safely maintain flight. The increase in camber also increases the wing drag, which can be beneficial during approach and landing, because it allows the aircraft to descend at a steeper angle.

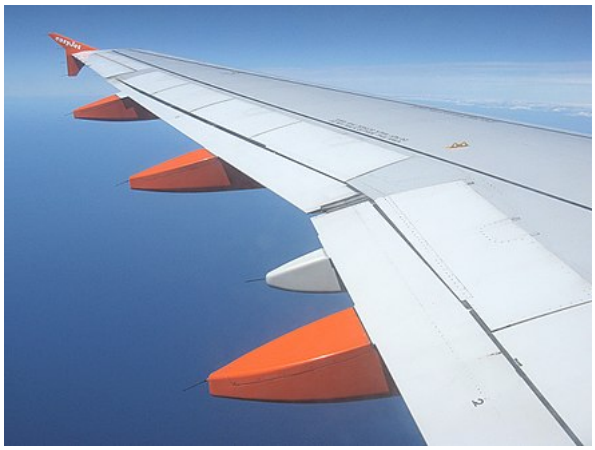

Figure 12: Example of real flaps: Easyjet A319

There are many different designs of flaps, with the specific choice depending on the size, speed and complexity of the aircraft on which they are to be used, as well as the era in which the aircraft was designed. Plain flaps, slotted flaps, and Fowler flaps are the most common. Krueger flaps are positioned on the leading edge of the wings and are used on many jet airliners.
The Fowler, Fairey-Youngman and Gouge types of flap increase the wing area in addition to changing the camber. The larger lifting surface reduces wing loading, hence further reducing the stalling speed.

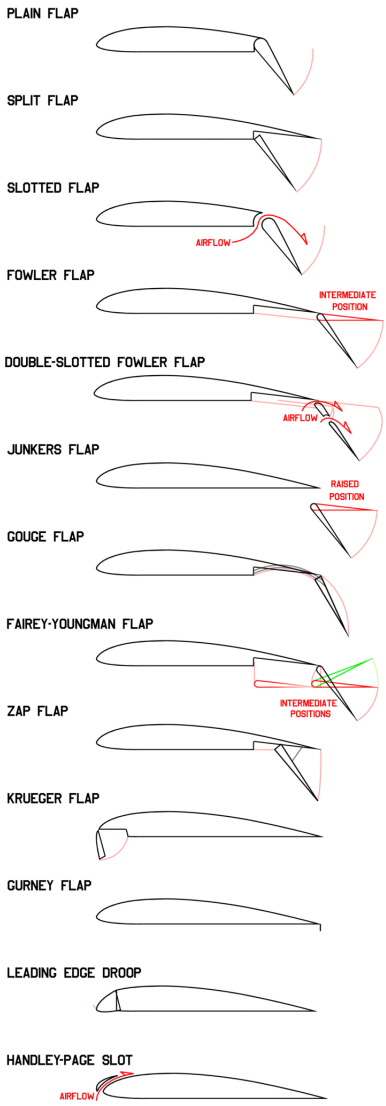

Figure 13: Different types of flaps

In this project the effect of the flaps is considered to be decoupled from the one of the elevator so as to apply two different controllers, one to the equation of the pitch angle, as described above, and the second one to adjust the plane altitude $z(t)$.
It follows that the flaps are able to control only $z(t)$ (and indirectly also z_{wr} and z_{wf}) and the do not affect the pitch angle.
In this way it is possible to use again the same technique of the feedback linearization plus PID, as it has been done for the elevator control in the previous section.

The equation for the lift force is the following

$$L = \frac{1}{2}\rho V^2 S C_L \tag{32}$$

where

1. L is the amount of lift produced,
2. ρ is the air density,
3. V is the speed of the aircraft relative to the air mass through which it is flying, namely the True airspeed
4. S is the area of the wing
5. C_L is the lift coefficient, which is determined by the shape of the airfoil used and the angle at which the wing meets the air (or angle of attack).

It follows that, the real effect of the flaps consists in increasing and decreasing the surface of the wing S and in part also the lift coefficient.
As written in (8) the equation related to the center of mass altitude is

$$\ddot{z} = f(z, z_{wf}, z_{wr}, \dot{z}, \dot{z}_{wf}, \dot{z}_{wr}) + L \tag{33}$$

where $f = \frac{1}{M}\left[-k_r(z - z_{wr}) - k_f(z - z_{wf}) - c_r(\dot{z} - \dot{z}_{wr}) - c_f(\dot{z} - \dot{z}_{wf})\right]$ and L is an acceleration if divided by the airplane mass M.
By applying the exact same procedure as it has been done for the control of the pitch angles, one might end up with an error dynamics for the airplane altitude

$$\ddot{e}_z + K_d\dot{e}_z + K_p e_z + K_i \int_0^t e(\tau)_z d\tau = 0 \tag{34}$$

where $e_z = z - z_d$.
However in this case, the main focus of the control problem is to control the descent speed rather than the altitude of the airplane. As a matter of fact the proportional gain K_p can be set to zero, so as to obtain a velocity error dynamics.
However the feedback on the altitude is necessary in the landing maneouver, indeed the altitude is "observed" by a boolean variable inside the simulink file, which activates when the rear gear touch the ground.
In general the desired descent velocity is a constant value about $1 - 2$ m/s, so as the altitude starts to decrease linearly when the steady-state value for the velocity is reached up, this fact justify the omission of a desired altitude inside the controller specifications.

5 Suspension Variational Feedback Control

The last input given to the system consists in the control of the semi-active suspension placed in the front landing-gear. In particular the control problem, in this case, is to find the optimal value of the damping coefficient c_f with the aim of making the oscillations fade as much as possible. As a matter of fact, especially at the instant the plane lands, the forces transmitted from the ground to the nose of the airplane can grow of several orders of magnitude, so that a good choice of the damping coefficient becomes a necessary condition to obtain a comfortable landing for the passengers. Moreover, also in the case of other maneuvers such as taxiing, the damping coefficient inside the suspension in very useful to yield the airplane movements as smooth as possible.
Differently from the previous controllers, in place of using a linear controller or a feedback linearization, in the following, the variational feedback controller (VFC) will be analyzed and implemented to solve the semi-active suspension control problem.
The latter is indeed a new method for feedback control of nonlinear systems and it has been introduced in [1], where, starting from the variational control theory, the controller is developed.

5.1 Theoretical Background

Given a dynamic system

$$\dot{x} = f(x, u, t) \tag{35}$$

the general idea behind the optimal control via variational approach is to find the state vector x and the otpimal control u that minimize a given cost function

$$J = \int_{t_0}^{t_f} L(x, u, t)dt \tag{36}$$

The solution is based on the Pontryagin principle and the Euler-Lagrange approach, and it is often restricted to some special conditions that simplify the problem, such as the linearity of the cost index, which yield to the well-known Linear Quadratic Regulator (LQR).
With the addition of the Lagrangian multipliers λ and of a penalty function $P(u)$, the solution of problem can be reformulated in an elegant way as follows:

$$\begin{cases} L_x^T - \dot{\lambda}^T - \lambda^T f_x = 0 \\ L_u^T - \lambda^T f_u - P_u = 0 \\ \dot{x} = f(x, u, t) \\ x(t_0) = x_{t_0} \\ \lambda^T(t_f)\delta x(t_f) = 0 \end{cases} \tag{37}$$

Despite being very well-posed, the problem above is quite difficult to solve. It needs indeed the *program of control* which is characterized by an open-loop strategy. Therefore, in [1], the problem is then reduced to a special class of objective function, in order to maintain the nonlinear nature of the function f, while solving it as a pure feedback control. The technique used is called Variational Feedback Controller (VFC).
The hypothesis on the objective function L is that it must depend on the variables x and u only trough $\dot{x} = f(x, u, y)$, where $y(t)$ is the external disturbance. Moreover the penalty function $P(u)$

is removed from the integral.

$$\begin{cases} J = \int_{t_0}^{t_f} L(f(x,u,y),y)dt \\ \dot{x} = f(x,u,y) \\ x(t_0) = x_{t_0} \end{cases} \tag{38}$$

where, here and in the following $u \in U \subset \mathbb{R}^p$. It follows that if the optimal control $u^* \in U$ then the actual control $u = u^*$, else if $u^* \notin U \longrightarrow u = u_{\partial U}$, where $u_{\partial U}$ is the value of the control on the boundary of U "closest" to u^*.
The problem stated in this way leads to the following system of Euler-Lagrange equations and transversality conditions:

$$\begin{cases} (L_f - \lambda)^T f_x - \dot{\lambda}^T = 0 \\ (L_f - \lambda)^T f_u = 0^T \\ \dot{x} = f(x,u,y) \\ x(t_0) = x_{t_0} \\ \lambda^T(t_f)\delta x(t_f) = 0 \end{cases} \tag{39}$$

which is a simplified version of (37). However a general closed-form solution still cannot be found, then a further simplification needs to be done.
Suppose the state vector and the control input have the same dimension, i.e. $n = p$, it follows that f_u is a square matrix. If f_u is non-singular, from the system of equation (39) it follows that

$$L_f - \lambda = 0 \tag{40}$$

hence

$$\dot{\lambda} = 0 \tag{41}$$

Taking into account also the transversality condition, if follows that

$$\lambda(t) = 0 \tag{42}$$

Being the Lagrangian multiplier equal to zero, the system (39) can be reduced to a new one, composed of only two equations

$$\begin{cases} L_f(f(x,u,y),y) = 0 \\ \dot{x} = f(x,u,y) \end{cases} \tag{43}$$

In conclusion, if x and y are measured by sensors at the time instant t, the optimal control value can be found by solving $L_f(f(x,u,y),y) = 0$, while the dynamic equation $\dot{x} = f(x,u,y)$ is used to make the system evolve according to the input previously found.
In a real-case scenario, it is quite rare that the number of input is equal to the number of state variables (i.e. $p < n$), hence f_u is a rectangular matrix of p columns and n rows. It follows that there exist infinite vectors $L_f - \lambda$ which satisfy the condition $(L_f - \lambda)^T f_u = 0^T$. The choice of $L_f - \lambda = 0$ for simplicity, implies that, since $n > p$, there are more conditions to be satisfied than the number of available control variables u, so in principle the problem can be solved only in a minumum error framework or under some constraints on the the function L. In particular, for a mechanical system of N_{DOF} degress of freedom the dimension of the state n, which is the same of the total number of equation is $2 \times N_{DOF}$, being 2 the maximum order of the derivatives involved. If the constraints on L are introduced, then a number N_{ID} of pair of equations of the system $L_f(f(x,u,y),y) = 0$ degenerate into a single repeated equation, still producing an exact

solution if $p = n - N_{ID}$.
Assume

$$L(f, y) = f^T A f + f^T B y \tag{44}$$

From $L_f(f(x, u, y), y) = 0$ it follows

$$(A + A^T) f(x, u, y) + By = 0 \tag{45}$$

with $f \in \mathbb{R}^n$, $A \in \mathbb{R}^{n \times n}$, $y \in \mathbb{R}^m$ and $B \in \mathbb{R}^{n \times m}$.
Moreover, it is reasonable to assume that the nonlinear dynamics is in the control affine form, namely

$$f(x, u, y) = \psi(x, y) + S(x, y)u \tag{46}$$

with $\psi \in \mathbb{R}^n$ and $S \in \mathbb{R}^{n \times p}$.
From (45) it follows that

$$\tilde{A} S(x, y) u = -\tilde{A} \psi(x, y) - By \tag{47}$$

with $\tilde{A} = A + A^T \in \mathbb{R}^n$ and $\tilde{A} S(x, y) \in \mathbb{R}^{n \times p}$.
Eventually, the over-determined solution of the optimal control problem is

$$u = \left[\tilde{A} S(x, y) \right]^{\#} \left[-\tilde{A} \psi(x, y) - By \right] \tag{48}$$

However, if some special conditions on A and B are satisfied, an exact solution for u can be obtained.
Suppose that $n = k \times p$ and $m = h \times p$, then $\tilde{A}$ can be decomposed using K^2 blocks, each of them made by a matrix $\tilde{A}_{ri}$ having dimension p^2, hence equation (47) becomes:

$$\sum_{i=1}^{k} \tilde{A}_{ri} S_i u = -\sum_{i=1}^{k} \tilde{A}_{ri} \psi_i - \sum_{j=1}^{h} B_{rj} y_j \tag{49}$$

The latter represents an explicit system of k matrix equations for $r = 1, 2, \ldots, k$ in terms of the single variable u. A partition has been introduced also for the rectangular matrix S using a number of k square matrices S_i having dimensions p^2, as well as for y partitioned using h sub-vectors of length p .
Pre-multiplying the previous equation by $\tilde{A}_{ri}^{-1}$, assumed to be non-singular, one obtains:

$$I S_1 u + \sum_{i=2}^{k} \tilde{A}_{r1}^{-1} \tilde{A}_{ri} S_i u = -\psi_1 - \sum_{i=2}^{k} \tilde{A}_{r1}^{-1} \tilde{A}_{ri} \psi_i - \sum_{j=1}^{h} \tilde{A}_{r1}^{-1} B_{rj} y_j \tag{50}$$

As it has been anticipated before, a possible chance in order to solve exactly all the written equations for any r, is to collapse all of them into a single identical equation. This requires simply that the sub-matrices satisfy the conditions:

$$\begin{cases} \tilde{A}_{p1}^{-1} \tilde{A}_{pi} = \tilde{A}_{11}^{-1} \tilde{A}_{1i}, & p = 2, ..., k; \quad i = 2, ..., k \\ \tilde{A}_{p1}^{-1} \tilde{B}_{pj} = \tilde{A}_{11}^{-1} \tilde{B}_{1j}, & p = 2, ..., k; \quad j = 1, ..., h \end{cases} \tag{51}$$

In conclusion, the solution of the optimal control problem is

$$u = \left(I S_1 + \sum_{i=2}^{k} \tilde{A}_{r1}^{-1} \tilde{A}_{ri} S_i \right)^{-1} \left(-\psi_1 - \sum_{i=2}^{k} \tilde{A}_{r1}^{-1} \tilde{A}_{ri} \psi_i - \sum_{j=1}^{h} \tilde{A}_{r1}^{-1} B_{rj} y_j \right) \tag{52}$$

Note that, the total number of independent coefficients of the symmetric matrix $\tilde{A}$ is $\frac{n^2+n}{2}$, the total number of independent coefficients of the matrix B is $n * m$, hence the previous conditions introduce $p^2(k-1)^2 + p^2(k-1)h$ restraints between these coefficients. This fact implies that there is a number of degrees of freedom in the choice of the objective function L, which is given by the difference between the number of independent coefficients and the number of the restraints. The latter is exactly the number of tunable parameters available in the design of the controller.

6 Simulation setting

In the following we will describe the setting in which the simulations of our approach have been tested. In particular a deep analysis on the landing scenario will be computed in order to point out the main challenges of every step of this complicated maneuver, putting in light for each phase the more relevant control input and its role in the scenario.

6.1 Landing Scenario

The landing is a transition from flying to taxiing and the landing maneuver is schematized in fig. (1). In its initial phase, flaps are used to permit a lower-approach speed and a steeper angle of descent. The airspeed and rate of descent are stabilized, and the airplane is aligned with the runway centerline as the final approach is begun. When the airplane descends across the threshold of the runway, power is reduced further and the rate of descent and airspeed are slowed down by the flaps controller. The airplane is kept aligned with the center of the runway mainly by use of the rudder.
The objective of the control problem is to keep the airplane safely flying just a few meters above the runway's surface until it loses flying speed. In this condition, the airplane's rear wheels will strike the runway with a gentle bump. With the wheels of the rear landing gear firmly on the runway, the elevator control enters the loop joint with the flaps. The elevator controller holds the airplane in a nose-high attitude which keeps the front wheel from touching the runway until forward speed is much slower. The purpose here is to avoid overstressing and damaging the nose gear when it touches down on the runway.
Once both the gears have touched the ground, and the airplane speed is continuing to decrease, the VFC controller is activated in order to control the damping coefficient of the front wheel, so as to flatten the airplane oscillations and to guarantee a smooth as possible landing for the passengers, the landing maneuver is considered complete when the airplane horizontal velocity reaches its steady state value.

6.2 Parameters numerical values

In this section we gather all the parameters used during this project, starting from the numerical values of the model, referring to an A320 model as in [4], to the control gains and the numerical values used for the VFC controller.

Quantity	Symbol	Value	S.I.
Length	L	12.6	[m]
Front-c.o.m.	L_f	11.34	[m]
Rear-c.o.m.	L_r	1.26	[m]
Mass	M	73000	[kg]
Mass on rear gear	m_r	65700	[kg]
Mass on front gear	m_r	7300	[kg]
Inertia moment	J_y	3.3×10^5	[kg m^2]

Quantity	Symbol	Value	S.I. Unit
Wheel Radius	R_t	0.5	[m]
Front spring coeff.	k_f	$1e^6$	[N/m]
Rear spring coeff.	k_f	$1e^6$	[N/m]
Front Gear Mass	m_{tf}	120 $\times 2$	[kg]
Rear Gear Mass	m_{tf}	120 $\times 8$	[kg]
Rear damping coeff.	c_r	5.12 $\times 10^5$	[Ns/m]
Front gear inertia	J_f	30	[Kgm^2]
Rear gear inertia	J_f	120	[Kgm^2]

Quantity	Symbol	Value	S.I. Unit
Proportional gain (θ)	Kpθ	5	
Integral gain (θ)	Kiθ	3	
Derivative gain (θ)	Kiθ	3	
Desired pitch angle	θ_d	4;0	[°]

Quantity	Symbol	Value	S.I. Unit
Proportional gain (L)	Kp_L	1000	
Integral gain (L)	Ki_L	10	
Derivative gain (L)	Ki_L	100	
Desired vertical velocity	$\dot{z}_d$	-1	[m/2]
Lift Coefficient	c_d	2	[m/2]
Drag Coefficient	c_d	0.35	[m/2]
Air density	ρ_{air}	1.18	[kg/m^3]
Max. Flap area	Af_{max}	300	[m^2]
Min. Flap area	Af_{max}	100	[m^2]

The VFC is applied to the front gear of the airplane, since the control input c_f acts of this specific subsystem, which is schematized in the following figure

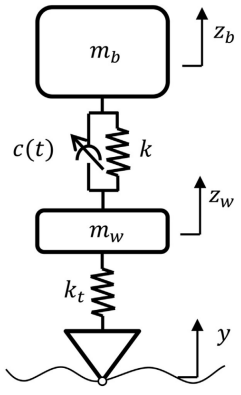

Figure 14: 2-d.o.f. Suspension Model

As it has been deeply analyzed in [1], by applying (52) to the suspension system, yields to the following non-linear control law

$$c_f^* = \tilde{g}_0 \frac{f_{el}(z - zwf)}{f_{da}(\dot{z} - z\dot{w}f)} + \tilde{g}_1 \frac{f_{el}(zwf - r_f)}{f_{da}(\dot{z} - z\dot{w}f)} + \tilde{g}_2 \frac{\dot{z}}{f_{da}(\dot{z} - z\dot{w}f)} + \tilde{g}_3 \frac{z\dot{w}f}{f_{da}(\dot{z} - z\dot{w}f)} + \tilde{g}_4 \frac{r_f}{f_{da}(\dot{z} - z\dot{w}f)} \quad (53)$$

where the gains are the tuning parameters of the controller, except for $\tilde{g}_0$ which is fixed:

1. $\tilde{g}_0 = -k_f$
2. $\tilde{g}_1 = \dfrac{\tilde{a}_{13} k_{tf}}{\tilde{a}_{11} m_f \left(\dfrac{\tilde{a}_{13}}{\tilde{a}_{11} m_f} - \dfrac{1}{m_{tf}} \right)}$
3. $\tilde{g}_2 \dfrac{-\tilde{a}_{12}}{\tilde{a}_{11} \left(\dfrac{\tilde{a}_{13}}{\tilde{a}_{11} m_f} - \dfrac{1}{m_{tf}} \right)}$
4. $\tilde{g}_3 = \dfrac{-\tilde{a}_{14}}{\tilde{a}_{11} \left(\dfrac{\tilde{a}_{13}}{\tilde{a}_{11} m_f} - \dfrac{1}{m_{tf}} \right)}$
5. $\tilde{g}_4 = \dfrac{-b}{\tilde{a}_{11} \left(\dfrac{\tilde{a}_{13}}{\tilde{a}_{11} m_f} - \dfrac{1}{m_{tf}} \right)}$

The a_{ij} and b coefficients correspond to different choices of the matrices $\tilde{A}$ and B, where the first has dimension 4×4 since $N_{DOF} = 4$, while B collapses into the scalar b.
The condition in (51) can be written in this case as:

- $\dfrac{\tilde{a}_{12}}{\tilde{a}_{11}} = \dfrac{\tilde{a}_{22}}{\tilde{a}_{21}} = \dfrac{\tilde{a}_{32}}{\tilde{a}_{31}} = \dfrac{\tilde{a}_{42}}{\tilde{a}_{41}}$
- $\dfrac{\tilde{a}_{13}}{\tilde{a}_{11}} = \dfrac{\tilde{a}_{23}}{\tilde{a}_{21}} = \dfrac{\tilde{a}_{33}}{\tilde{a}_{31}} = \dfrac{\tilde{a}_{43}}{\tilde{a}_{41}}$
- $\dfrac{\tilde{a}_{14}}{\tilde{a}_{11}} = \dfrac{\tilde{a}_{24}}{\tilde{a}_{21}} = \dfrac{\tilde{a}_{34}}{\tilde{a}_{31}} = \dfrac{\tilde{a}_{44}}{\tilde{a}_{41}}$

By applying these condition one might also re-write the equation for the optimal value of the from damping coefficient by substituing them into (53).

6.3 Sensors and State Estimation

Flight instruments are the instruments in the cockpit of an aircraft that provide the pilot with data about the flight situation of that aircraft, such as altitude, airspeed, vertical speed, heading and much more other crucial information in flight. They improve safety by allowing the pilot to fly the aircraft in level flight, and make turns, without a reference outside the aircraft such as the horizon. The sensors useful and available in most of airplanes are summarized in the following:

1. Altimeter: it shows the aircraft's altitude above sea-level by measuring the difference between the pressure in a stack of aneroid capsules inside the altimeter and the atmospheric pressure obtained through the static system. The most common unit for altimeter calibration worldwide is hectopascals (hPa), except for North America and Japan where inches of mercury (inHg) are used. The altimeter is adjustable for local barometric pressure which must be set correctly to obtain accurate altitude readings, usually in either feet or meters.

2. Airspeed indicator: it shows the aircraft's speed relative to the surrounding air. Knots is the currently most used unit, but kilometers per hour is sometimes used instead. The airspeed indicator works by measuring the ram-air pressure in the aircraft's Pitot tube relative to the ambient static pressure. The indicated airspeed (IAS) must be corrected for nonstandard pressure and temperature in order to obtain the true airspeed (TAS). The instrument is color coded to indicate important airspeeds such as the stall speed, never-exceed airspeed, or safe flap operation speeds.

3. Vertical speed indicator: The VSI (also sometimes called a variometer, or rate of climb indicator) senses changing air pressure, and displays that information to the pilot as a rate of climb or descent in feet per minute, meters per second or knots.

4. The attitude indicator (also known as an artificial horizon) shows the aircraft's relation to the horizon. From this the pilot can tell whether the wings are level (roll) and if the aircraft nose is pointing above or below the horizon (pitch). Attitude is always presented to users in the unit degrees (°). The attitude indicator is a primary instrument for instrument flight and is also useful in conditions of poor visibility.

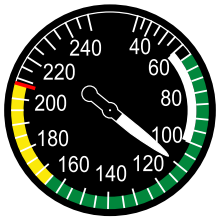

Figure 15: Airspeed indicator (V_x)

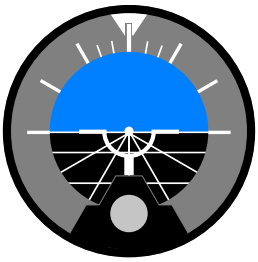

Figure 16: Attitude indicator (θ)

Figure 17: Altimeter (z)

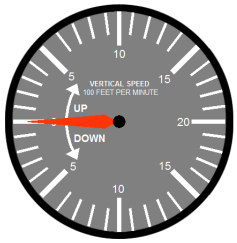

Figure 18: Vertical speed indicator ($\dot{z}$)

Referring to the airplane model, the state vector is the following

$$x(t) = \begin{bmatrix} z \\ z_w f \\ z_w r \\ \theta \\ \dot{z} \\ \dot{z}_{wf} \\ \dot{z}_{wr} \\ \dot{\theta} \end{bmatrix} \tag{54}$$

which is augmented with the variables connected to the horizontal direction and the wheels angular position and velocity.

$$x_p(t) = \begin{bmatrix} x \\ \theta_r \\ \theta_f \\ \dot{x} \\ \omega_r \\ \omega_f \end{bmatrix} \tag{55}$$

It can be noted that the sensors available among the flight instruments are not able to cover all the state information. More precisely, the sensors can measure z, $\dot{z}$, θ, $\dot{\theta}$ and the horizontal velocity v_x. Moreover, sensors are always affected from disturbance and noise, this means that an observer or a state estimator is necessary in order to implement the controllers proposed in the previous sections. In particular, we have decided to use an Extended Kalman Filter (EKF) to estimate the wheels position z_{wf} and z_{wr} and their velocities $\dot{z}_{wf}$ and $\dot{z}_{wr}$, and to clean the sensors data from the disturbance.
Regarding the subsystem composed of the equations 16, 17 and 18, no estimation is needed. As a matter of facts, the wheel angular velocities and position can be easily measured through the encoders mounted inside the structure of the gears, while the horizontal position can be obtained from the ground station data and also from the landing strip, so the EKF is used only to clean the data from the noise.
Hence, the state measurement and estimation is summed up as follows

$$\textit{EKF: from sensors output} \quad \begin{cases} \begin{bmatrix} z \\ \theta \\ \dot{z} \\ \dot{\theta} \\ x \\ v_x \\ \theta_f \\ \theta_r \\ \omega_f \\ \omega_r \end{bmatrix} \end{cases} \tag{56}$$

$$\textit{EKF: completely estimated} \quad \begin{cases} \begin{bmatrix} z_{wf} \\ z_{wr} \\ \dot{z}_{wf} \\ \dot{z}_{wr} \end{bmatrix} \end{cases} \tag{57}$$

where the output variables in (56) are cleaned from the disturbance by the EKF after the measurements.
In the following figure are reported the results on the estimation of z_{wf} and z_{wr} computed by the EKF.

Figure 19: EKF Results

7 Simulation results

To validate the proposed approach, we performed several simulations in the setting described in the previous section. In this section are reported the results we have obtained simulating the landing covering all the three phases. In figure (20), the are reported the evolution of the main variables of interest, namely z, θ, z_{wf} and z_{wr}.

Figure 20: State variables $[z, \theta, z_{wf}, z_{wr}]$

The first thing that can be noted is that the rate of descendent in the first phase of the landing is quite low, as desired. This facts is due to the implementation of the controllers on the flaps and the equilibrator.
From figure (21), it is explicit how the vertical velocity tends to the desired steady-state value of 1 m/s, yielding a very low descendent rate.

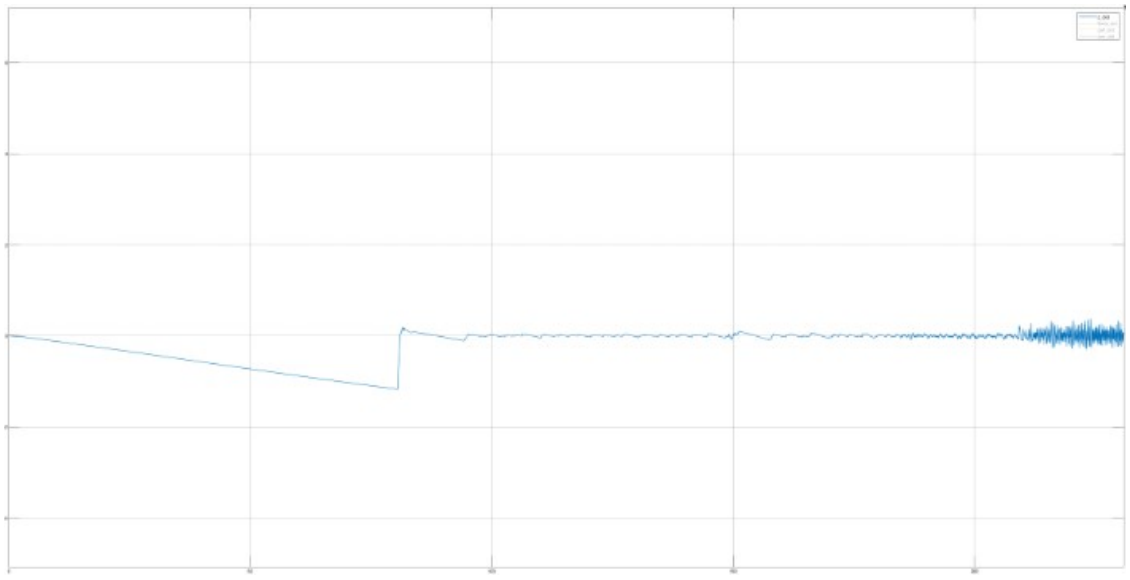

Figure 21: vertical velocity $\dot{z}$

Moreover, from figure (23), it can be seen how the evolution of the pitch angle θ, follows the two desired position. In the runway approach phase, it stabilizes near to $4 - 5$ degrees, while as soon as the rear gear touches the ground, the controller reacts immediately to move the angle to the zero value so as to maintain the plane horizontal with respect to the ground.

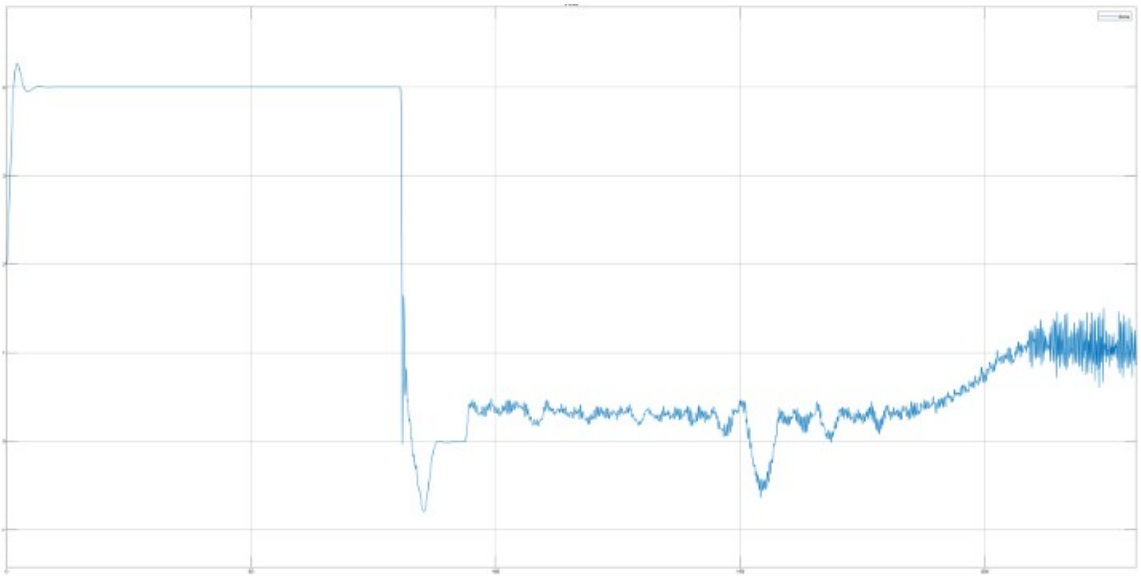

Figure 22: Pitch angle θ

The same fact described above can be found also by looking at the plots of the front and rear altitudes z_{wf} and z_{wr}. As a matter of facts, during the runway approach phase the nose of the airplane is above the rear of a few meters, in order to keep the airplane pitch angle to the desired value. Clearly, when the rear touches the ground, the front and the rear vertical position reach the same value, also shared by the altitude of the center of mass.

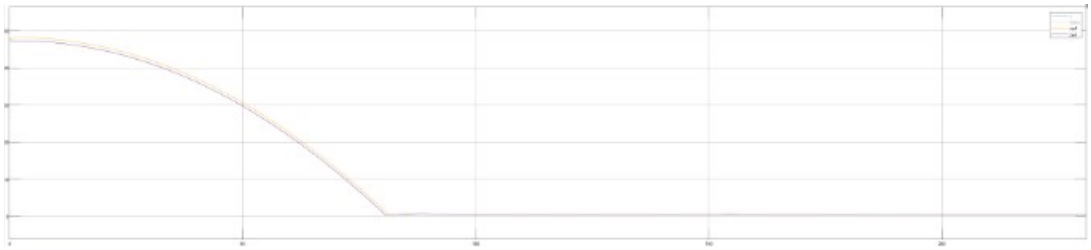

Figure 23: Gears altitude z_{wf} and z_{wr}

To conclude the analysis of the simulation, it is also necessary to observe the evolution of the horizontal velocity. From figure (24), it can be noted how v_x evolves in time. During the first phase, it decreases quite slowly, mainly because of the air brakes. It is important to point out that, these are not a control variable for our model, however we have tried to emulate their behaviour, by including them into the aerodynamic resistance F_{aereo}, which for this reason has been increased a bit with respect to the equation given in the previous sections.
The behaviour in the second phase, is affected by the Pacejka model. Indeed, due to the latter subsystem it is possible to decrease the horizontal velocity, by acting on the brake system of the gear, through the brake moments. As the airplane touch the ground, the system suddenly reacts to the forces trasmitted from it, and the changement on steep of the graph is evident.

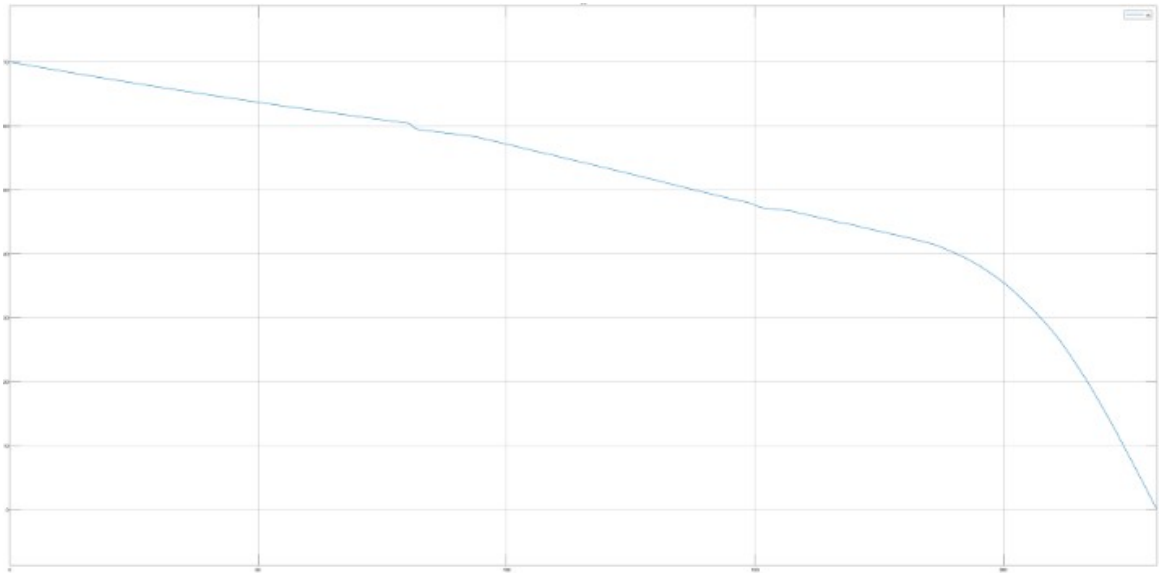

Figure 24: Horizontal velocity v_x

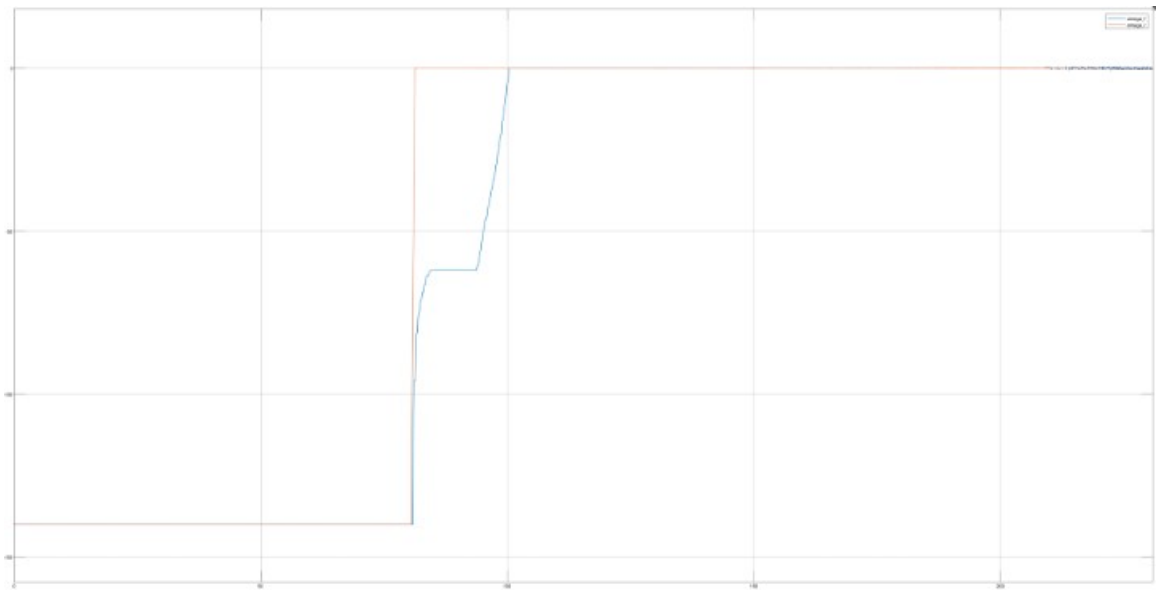

Figure 25: Wheels angular velocity ω_r and ω_f

Finally, it can be noted that the simulation stops as soon as the horizontal velocity is zero, meaning that the landing has been completed successfully, and the airplane stands still on the ground.

8 Conclusions

We would like to conclude this report by underlining some possibilities for future work on the project. In this project we have deeply analyzed the landing scenario and all the problems and maneuvers connected to it. We have implemented different control techniques through several control inputs, directly related to the real controllers of an airplane. However, our models includes some remarkable simplifications too. First thing first, the main approximation consists in studying the system as it was a planar problem. The latter is indeed a strong simplification, since the lateral forces acting on the plane can not be always be neglected, both because of the aerodynamics that act on the wings while flying and especially while maneuvering the gears wheels, where the lateral forces on them could change the model equations, for instance by inducing undesired gyroscopic effects. Moreover, one might argue that the control inputs could include some delays which can end-up affecting the stability of the entire system, for instance when using the PID controller after the Feedback Linearization. However, the study of this simulation is self-contained and valid for the purposes we were supposed to tackle at the beginning of the project.

Appendices

Here in the appendix we gather all the Simulink blocks, that we have created in order to perform all the simulations.

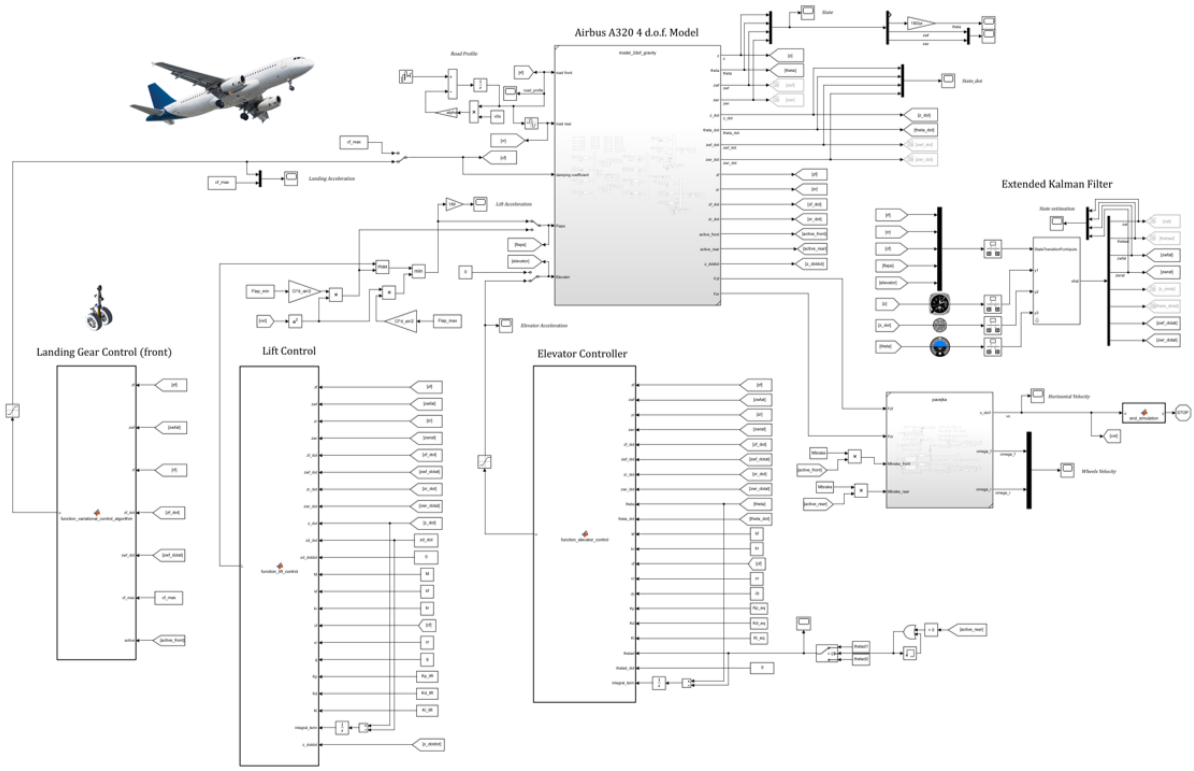

Figure 26: 7-d.o.f. model

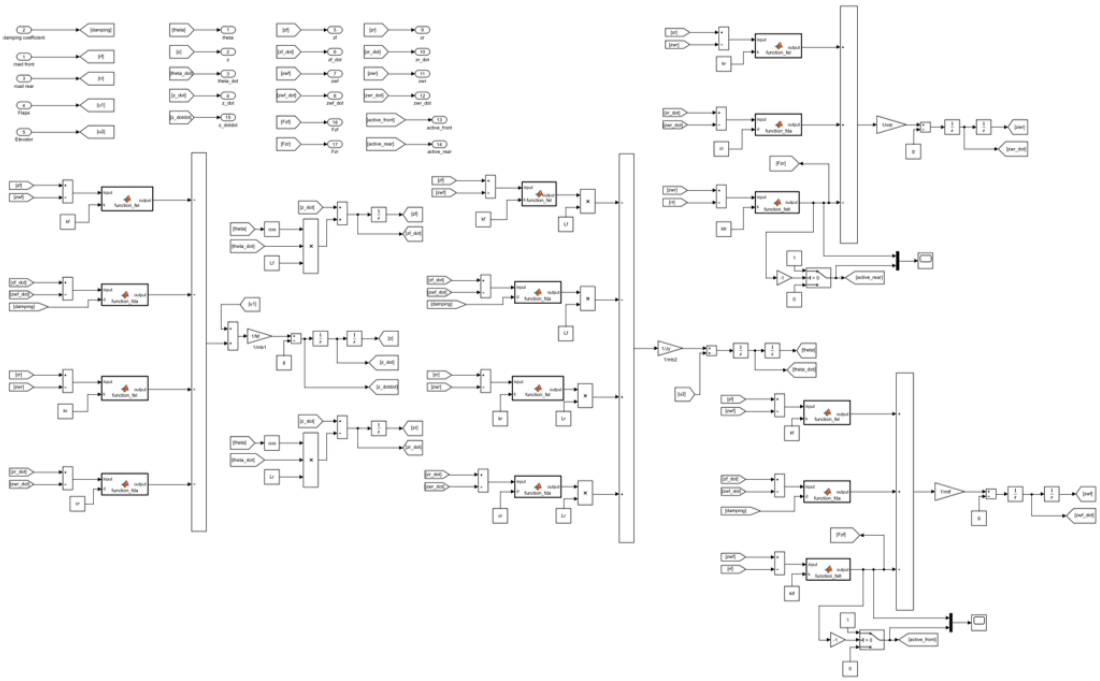

Figure 27: 4-d.o.f. model

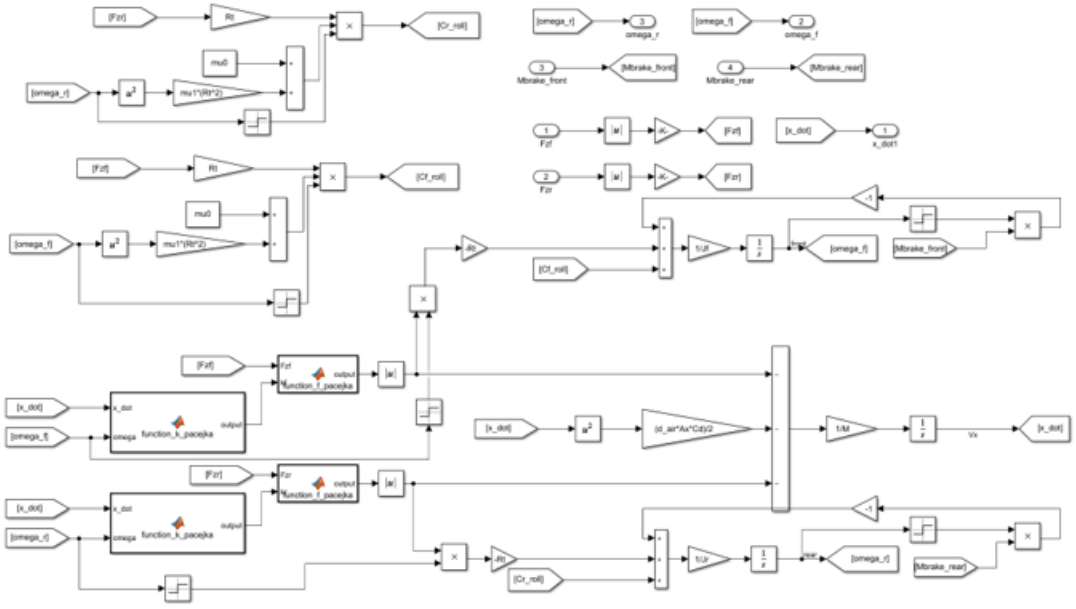

Figure 28: Pacejka model

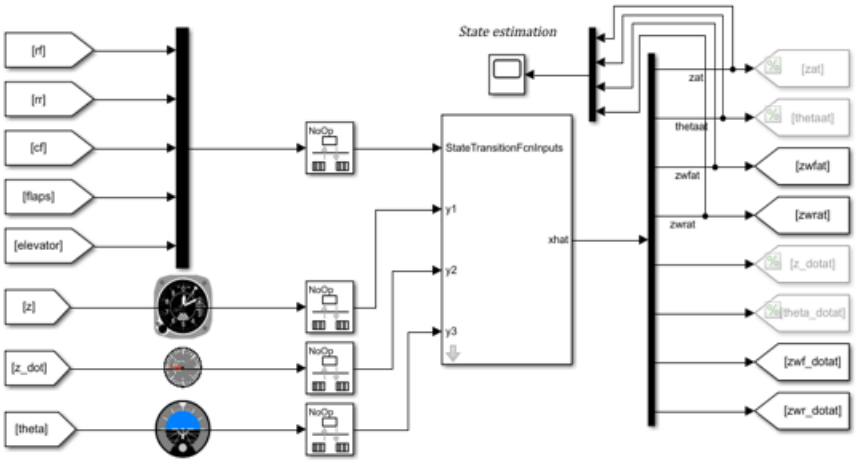

Figure 29: Extended Kalman Filter

References

[1] G. Pepe, A. Carcaterra (2016) VFC – Variational Feedback Controller and its application to semi-active suspensions, Mechanical Systems and Signal Processing, Volumes 76–77, 2016, Pages 72-92.

[2] Krüger, Wolf Morandini, Marco. (2008). Numerical Simulation of Landing Gear Dynamics: State-of-the-art and Recent Developments.

[3] Agostinacchio, M. Ciampa, Donato Olita, Saverio. (2013). The vibrations induced by surface irregularities in road pavements – a Matlab® approach. European Transport Research Review. 6. 267-275. 10.1007/s12544-013-0127-8.

[4] AIRBUS, Aircraft characteristics airport and maintenance planning, Revision n°39, Dec 01/20

[5] Ambalaparambil, Sanoopkumar, "Aircraft landing gear simulation and control" (2003). Thesis. Rochester Institute of Technology

[6] Pazmany, L.: Landing Gear Design for Light Aircraft. Vol 1. ISBN 0-9616777-0-8, 1986

[7] Roskam, J.: Airplane Design, Part IV: Layout Design of Landing Gear and other Systems, 1986

[8] Hitch, H.P.Y.: Aircraft ground dynamics, Vehicle System Dynamics 10, 1981, pp. 319–332.

[9] Zegelaar, P., Pacejka, H.: Dynamic tyre responses to brake torque variations. Vehicle System Dynamics Supplement, Vol. 27, pp. 65–79, 1997.

[10] Grossmann, D.T.: F-15 Nose Landing Gear Shimmy, Taxi Tests and Corrective Analyses. SAS Technical Paper 801239.

[11] URL: https://x-engineer.org/automotive-engineering/chassis/vehicle-dynamics/tire-model-for-longitudinal-forces/

[12] Besselink, I.J.M.: Shimmy of Aircraft Main Landing Gears. Doctoral Theses, TU Delft, Netherlands, 2000.

[13] Jocelyn L. Pritchard, An Overview ofLanding Gear Dynamics, NASA/TM-1999- 209143, ARL-TR-1976